M Ű E G Y E T E M 1 7 8 2
Budapest University of Technology and Economics
Faculty of Mechanical Engineering
Department of Hydrodynamic Systems

Instabilities of pressure relief valve systems

PhD Dissertation

Written by: Csaba Bazsó
M.Sc. in Mechanical Engineering

Supervisor: Dr. Csaba Hős
associate professor

3rd March 2014, Budapest

Contents

1 Mathematical modelling **5**
- 1.1 Introduction . . . 5
- 1.2 Approximations in adapting fluid and solid mechanical fundamentals . . . 6
- 1.3 Flow through a valve . . . 7
  - 1.3.1 Mass flow rate for incompressible turbulent flow . . . 8
  - 1.3.2 Mass flow rate for compressible, turbulent chocked flow . . . 8
- 1.4 Valve body dynamics . . . 9
- 1.5 Reservoir pressure dynamics . . . 11
  - 1.5.1 Reservoir pressure dynamics for compressible fluid . . . 11
  - 1.5.2 Reservoir pressure dynamics for incompressible fluid . . . 11
- 1.6 Pipeline dynamics . . . 11
  - 1.6.1 Incompressible flow . . . 12
  - 1.6.2 Compressible flow . . . 12
- 1.7 Model development, numerical solution techniques . . . 12
  - 1.7.1 Incompressible model: pipe–valve system . . . 13
  - 1.7.2 Compressible model: reservoir–pipe–valve system . . . 15
  - 1.7.3 Tools of quantitative and qualitative analysis . . . 17

2 Dynamic instability of a pipe–valve system **19**
- 2.1 Introduction . . . 19
- 2.2 Mathematical model of a pipe–valve system . . . 19
- 2.3 One-parameter study: effect of flow rate at fixed set pressure . . . 20
- 2.4 Two-parameter study: effect of set pressure . . . 25
- 2.5 Conclusion . . . 27
- 2.6 Contribution . . . 28

Chapter 1

Mathematical modelling

1.1 Introduction

In this section the mathematical model development of pneumatic and hydraulic pressure relief valve systems is presented. The two systems are shown in Figure 1.1. The left configuration

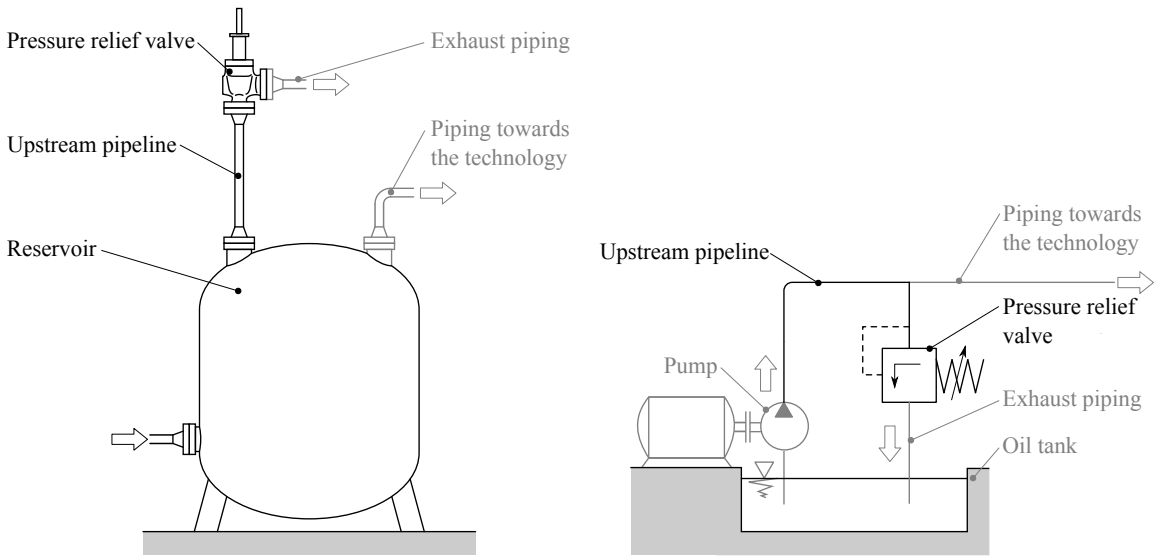

Figure 1.1: Examples for pressure relief valve installation. Left: Configuration typical of pneumatic supply systems or natural gas preparing systems. Right: Hydraulic power transmission system.

is typical of pneumatic supply systems or natural gas preparing systems. In such cases the pressure relief valve is installed onto the reservoir directly or via an upstream pipe. The right sketch represents the valve installation in a hydraulic power transmission system. The pressure relief valve is mounted into the system right after the volumetric pump via pipe.

The chapter is organised as follows. First, a brief overview is given about the employed solid and fluid mechanical approximations. Afterwards the flow and force conditions of the valve are introduced leading to the derivation of the valve body dynamics. Then the reservoir pressure

dynamics and fluid dynamics inside the pipeline is shown. Although the hydraulic system does not consist of reservoir, the derivation of the reservoir pressure dynamics is provided for liquid working medium as well. Based on the obtained governing equations, the mathematical model development and numerical solution techniques are presented for both the hydraulic and pneumatic valve systems. Finally, the tools of qualitative and quantitative analysis are introduced.

1.2 Approximations in adapting fluid and solid mechanical fundamentals

We employ fluid-structure interaction to explore the static and dynamic behaviour of the investigated valve systems. The elements of the systems and their components (reservoir, pipe, valve body, spring, seat) are approximated to be rigid bodies. The collision that may occur between the valve body and seat is supposed to follow the Newtonian restitution impact law occurring under an infinitesimal moment. The valve being a spring mass system is considered as a 1 DoF oscillatory system. On fluid part we deal with both compressible (gas working medium) and slightly compressible (e.g., hydraulic oil, water working medium) flows. In the case of compressible flow the fluid is assumed to be ideal and obey the ideal gas law. For slightly incompressible fluids we consider constant temperature ($T = \text{constant}$) and barotropic change of state, that is the density is only function of the pressure $\rho = \rho(p)$. Small disturbances in fluid velocity (v), pressure (p), and density (ρ) travel at the velocity of speed of sound given by

$$a = \sqrt{\frac{dp}{d\rho}} \tag{1.1}$$

(for detail see e.g., **?**, page 268). The compressibility of a liquid can be expressed by its *bulk modulus of elasticity* E. By definition (see **?**, page 16) the bulk modulus of elasticity is

$$E = -\frac{dp}{d\mathcal{V}/\mathcal{V}} \tag{1.2}$$

that simply states that the increase of the pressure dp will cause $-d\mathcal{V}$ volume change of any volume $\mathcal{V}$ of a liquid. In order to obtain convenient formulae for speed of sound and bulk modulus of elasticity we make some considerations. First, let us observe the slightly compressible fluids. Since

$$\frac{d\mathcal{V}}{\mathcal{V}} = -\frac{d\rho}{\rho} \tag{1.3}$$

the bulk modulus of elasticity can be rewritten as

$$E = \rho\frac{dp}{d\rho}. \tag{1.4}$$

Substituting (1.4) into (1.1) we have

$$a = \sqrt{\frac{E}{\rho}}. \tag{1.5}$$

In this work the pressure level and the change of its value is $\mathcal{O}(10^6)$ of order of magnitude while the bulk modulus of the hydraulic oil is $\mathcal{O}(10^9)$. Let us determine the order of the density change employing (1.2) and (1.3) we have

$$\frac{d\mathcal{V}}{\mathcal{V}} = -\frac{dp}{E} = \mathcal{O}(10^{-3}) \tag{1.6}$$

which is negligible. After introducing the sonic velocity that allows the formation of waves and the bulk modulus describing the compressibility of the fluid, it is common simplification in fluid mechanics to assume constant density and considering the slightly compressible fluid to be incompressible. Later on we shall refer to liquid as incompressible fluids and calculate the speed of sound and the bulk modulus of elasticity vica versa based on (1.5).

Gas working medium is considered to be compressible and in this work it is supposed to obey the ideal gas law, that is

$$\frac{p}{\rho} = RT. \tag{1.7}$$

being R the specific gas constant. Assuming the process to be reversible and adiabatic, the process can be considered isentropic,

$$\frac{p}{\rho^\kappa} = \text{constant} \tag{1.8}$$

being κ the heat capacity ratio. Compounding (1.7) and (1.8) we obtain

$$a = \sqrt{\kappa RT} \tag{1.9}$$

that shows that the speed of sound is function of the absolute temperature only.

1.3 Flow through a valve

Let us consider a poppet valve with a conical valve body and sharp seat as illustrated in Figure 1.2. The fluid flows upwards in the passage and exits to the outlet through the gap between the poppet and the sharp seat. Let ϕ denote the half cone angle of the poppet, D_s the seat diameter, x_v the lift of the valve body, and $h = x_v \sin\phi$ the gap between the poppet and the seat. The cross-section of the passage on the upstream-side of the valve is uniform and identical to the cross-section of the seat ($A_s = D_s^2\pi/4$), while the gap area (often referred to in the literature as *vena contracta* or flow-through area) $A_g(x)$ for small lifts can be calculated as

$$A_g(x_v) = D_s\pi h = D_s\pi \sin\phi\, x_v := c_1 x_v, \qquad c_1 = D_s\pi\sin\phi. \tag{1.10}$$

For detailed deduction of (1.10) see Appendix **??**. Increasing the half cone angle up to $\phi = 90°$ we obtain a disk valve thus the flow-through area forms an annulus between the seat and the valve disk.

When dealing with compressible flow mass flow rate $\dot{m}$ is employed to quantify the flow, while for slightly compressible fluid (liquid), flow rate Q is used. The velocity on the upstream-side and through the gap are $v_{fl,s}$ and $v_{fl,g}$, respectively. The subscript s refers to the seat area while g for the gap area with which the fluid velocity is calculated from the (mass) flow rate.

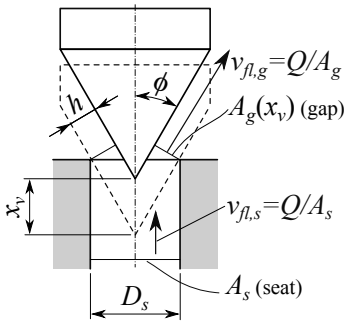

Figure 1.2: Representation of the geometrical quantities of the valve. The valve displacement is x_v, the diameter and the cross-section area of the inlet is denoted by D_s and A_s, respectively. h denotes the length of the gap while A_g stands for the gap area.

1.3.1 Mass flow rate for incompressible turbulent flow

The flow rate Q for incompressible turbulent flow through the poppet valve is given by the usual discharge formula (see e.g., Kasai (1968))

$$Q = C_d A_g(x_v)\sqrt{\frac{2\Delta p}{\rho}}, \quad \text{with} \quad \Delta p = p_v - p_0 \tag{1.11}$$

where C_d is the discharge coefficient, p_v and p_0 are the absolute pressure at the upstream and downstream side of the poppet valve, respectively, and ρ is the density of the working medium. The mass flow rate in a simplified form is then

$$\dot{m} = \rho Q = C_d A_g(x_v) c_2 \sqrt{\rho \Delta p}, \quad \text{with} \quad c_2 = \sqrt{2}. \tag{1.12}$$

1.3.2 Mass flow rate for compressible, turbulent chocked flow

In gas valves where significant pressure difference is between the upstream and downstream side it is reasonable to assume that the pressure difference is large enough for choked flow to occur. This means that flow reaches the sonic velocity at the *vena contracta* and hence the downstream pressure does not affect the flow rate; for details, see Zucrow and Hoffman (1976). As an illustration to quantify when this assumption is value, for the case of air whose specific heat capacity ratio is $\kappa = c_p/c_v = 1.4$, choked flow occurs if the pressure ratio reaches (see also Zucrow and Hoffman (1976))

$$\frac{p_v}{p_0} \geq \left(\frac{\hat{\kappa}+1}{2}\right)^{\left(\frac{\hat{\kappa}}{\hat{\kappa}-1}\right)}\Bigg|_{\hat{\kappa}=1.4} \geq 1.8929. \tag{1.13}$$

Now consider choked flow through an orifice with discharge coefficient C_d, absolute upstream pressure and density p_v and ρ_v, absolute downstream pressure p_0. Since $A_g(x_v) \ll A_s$ chocked flow occurs at the flow-through area. The mass flow rate for choked, compressible flow can be expressed as (see e.g. Zucrow and Hoffman (1976))

$$\dot{m} = C_d A_g(x_v)\, c_2 \sqrt{\rho_v\, p_v}, \tag{1.14}$$

where the constant c_2 is defined via

$$c_2 = \sqrt{\hat{\kappa}\left(\frac{2}{\hat{\kappa}+1}\right)^{\frac{\hat{\kappa}+1}{\hat{\kappa}-1}}}. \tag{1.15}$$

1.4 Valve body dynamics

To obtain the force exerted by the fluid we apply the momentum theory on the control volume cv, demonstrated in Figure 1.2. According Newton's second law, the sum of all external forces

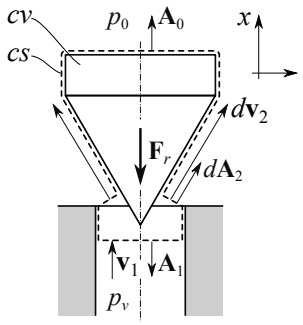

Figure 1.3: Momentum theory applied on the poppet. cs and cv denote the control surface and control volume. p_v and p_0 are the pressure at the upstream and downstream side. $\mathbf{A}_1$ and $\mathbf{A}_0$ denote the surface vectors of cs on the upstream side and downstream side while $\mathbf{A}_2$ is subset of $\mathbf{A}_0$ and depicts that segment of cs through which the fluid exits the control surface. $\mathbf{v}_1$ and $\mathbf{v}_2$ are the vectors of fluid velocity entering and leaving the control surface. $\mathbf{F}_r$ depicts the reaction force to hold the valve body in place. $|\mathbf{A}_1| = A_s$, $|\mathbf{A}_2| = A_{ft}$ while assuming uniform velocity at the inlet and the gap $|\mathbf{v}_1| = v_{fl,s}$ and $|\mathbf{v}_2| = v_{fl,g}$

on a control volume cv is equal to the time rate change of momentum within the control volume plus the net flux of momentum through the control surface cs.

$$\sum F = \frac{\partial}{\partial t}\int_{cv} \rho \mathbf{v} d\mathcal{V} + \int_{cs} \rho \mathbf{v}(\mathbf{v} \cdot d\mathbf{A}) \tag{1.16}$$

It is conventional in the corresponding literature (see e.g. Urata (1969); Takenaka (1964)) that only the pressure force, drag force, and reaction force (needed to hold the poppet in place) taken into account as external forces; gravity and buoyancy are neglected. Moreover, the time dependent term of the momentum force is also typically neglected even for unsteady cases. The control surface of the control volume is denoted by cs and divided into two main parts, the upstream- and downstream-side surface elements $\mathbf{A}_1$ and $\mathbf{A}_0$ ($cs = \mathbf{A}_1 \cup \mathbf{A}_0$).The fluid enters the control surface through the surface element given with $\mathbf{A}_1$ whose magnitude is equal to the seat area $|\mathbf{A}_1| = A_s$ and exits through the surface element $\mathbf{A}_2$ whose magnitude is identical to the gap area $|\mathbf{A}_2| = A_g(x_v)$. Note, $\mathbf{A}_2$ is only a subset of the downstream-side control surface ($\mathbf{A}_2 \subset \mathbf{A}_0$). The entering and leaving fluid velocity vector field $\mathbf{v}_1$ and $\mathbf{v}_2$ are assumed to be uniform thus $|\mathbf{v}_1| = v_{fl,s}$ and $|\mathbf{v}_2| = v_{fl,g}$. Moreover, as Urata (1969) pointed out the net force due to pressure distribution at the upstream and downstream side of the control volume can be

approximated uniform and are p_v and p_0, respectively. Applying these considerations (1.16) can be rewritten as follows

$$-\int_{cs} p\ d\mathbf{A} + \mathbf{F}_{dr} + \mathbf{R} = \int_{cs} \rho\, \mathbf{v}(\mathbf{v}\cdot d\mathbf{A}). \tag{1.17}$$

Negative sign of the first term signifies that the pressure acts on the control surface opposite to the direction of the surface vector. $\mathbf{F}_{dr}$ stands for the drag while $\mathbf{F}_r$ denotes the reaction force. The pressure force on the upstream- and downstream-side can be expressed simply by

$$P_1 = -\int_{cs} p_v\ d\mathbf{A_1} = A_s p_v, \quad \text{and} \quad P_2 = -\int_{cs} p_0\ d\mathbf{A_0} = -A_s p_0 \tag{1.18}$$

while the momentum flux terms entering and leaving the control surface can be assumed to be

$$I_1 = \int_{cs} \rho\, \mathbf{v}_1(\mathbf{v}_1\cdot d\mathbf{A}_1) = \rho v_{fl,s}^2\,(-A_s) = -\rho Q^2 \frac{1}{A_s} \tag{1.19}$$

and

$$I_2 = \int_{cs} \rho\, \mathbf{v}_2(\mathbf{v}_2\cdot d\mathbf{A}_2) = \rho v_{fl,g}^2\, A_g(x)\cos\phi = \rho Q^2 \frac{\cos\phi}{A_g(x)} \tag{1.20}$$

The drag force acts in the direction of the flow, it increases the reaction force, consequently it has positive sign. Substituting these terms and applying the notations for the valve being in focus (1.17) becomes

$$A_s(p_v - p_0) + F_{dr} - F_r = \rho Q^2 \left(-\frac{1}{A_s} + \frac{\cos\phi}{A_g(x)}\right), \tag{1.21}$$

from which the total force exerted by the fluid is

$$F_{fl} := A_s(p_v - p_0) + \rho Q^2 \left(\frac{1}{A_s} - \frac{\cos\phi}{A_g(x)}\right) + F_{dr} = F_r. \tag{1.22}$$

The valve itself consists of an inertial mass, the valve body, and a pre-compressed spring. International safety standards dictate that if the pressure upstream of the valve reaches the set pressure — that which is sufficient to overcome the spring pre-compression — then the valve must open as quickly as possible. Due to this fact no additional damping is designed for pressure relief valves beside the damping effect of the drag and the added mass effect of the fluid (see e.g., Khalak and Williamson (1997); Askari et al. (2013)). The motion of the valve body can be described as a single degree–of–freedom rigid body, with mass of m, and spring constant of s. The pre–compression of the spring will be denoted by x_0 while x_v stands for the displacement of the valve body. The governing equation is thus given by

$$m\ddot{x}_v + s(x_0 + x_v) = F_{fl}, \qquad \text{for } x_v > 0, \tag{1.23}$$

As is a common approximation in rigid body mechanics, we assume a Newtonian restitution impact law. While this approximation may be overly simplistic, any attempt at a more realistic law is likely to be problematic owing to the necessity of resolving the energy dissipated by the valve and its surrounding fluid during an impact event.

$$(x_v^+,\ v_v^+) = (0,\ -r\, v_v^-) \tag{1.24}$$

with v_v^- being the velocity immediately before the impact while x_v^+ and v_v^+ being the displacement and velocity immediately after the impact and r stands for the restitution coefficient. Note, the above derivation can also be applied for disc plate valves as the half-cone angle is set $\phi = 90°$.

1.5 Reservoir pressure dynamics

Let us consider a rigid reservoir of volume V. The mass flow rate entering and leaving the reservoir are $\dot{m}_{r,in}$ and $\dot{m}_{r,out}$. Then the imbalance between the constant inflow and outflow rates, results in change in the reservoir pressure. The reservoir pressure dynamics is obtained for compressible and incompressible working medium as follows.

1.5.1 Reservoir pressure dynamics for compressible fluid

We assume that the fluid is gas and obeys the ideal gas law, $p/\rho = RT$, and that the process in the reservoir is isentropic, $p/\rho^{\kappa} = \text{constant}$. Mass balance in the reservoir of volume V therefore gives

$$\frac{\mathrm{d}m_r}{\mathrm{d}t} = V\frac{\mathrm{d}}{\mathrm{d}t}\left(\rho_r(t)\right) = V\frac{\mathrm{d}}{\mathrm{d}t}\left(\frac{p_r(t)}{RT_r(t)}\right) = \dot{m}_{r,in} - \dot{m}_{r,out} \tag{1.25}$$

Given an ambient reference state p_0, T_0, the temperature can be related to the pressure via

$$T(t) = T_0\left(\frac{p_r(t))}{p_0}\right)^{\frac{\kappa-1}{\kappa}}, \tag{1.26}$$

which gives

$$\dot{p}_r = \kappa\frac{RT_0}{V}\left(\frac{p_r}{p_0}\right)^{\frac{\kappa-1}{\kappa}}\left(\dot{m}_{r,in} - \dot{m}_{r,out}\right) = \frac{a^2}{V}\left(\dot{m}_{r,in} - \dot{m}_{r,out}\right), \tag{1.27}$$

with $a = \sqrt{\hat{\kappa}RT}$ being the sonic velocity. We emphasise again that the sonic velocity in the reservoir depends on temperature, which – as described by (1.26) – changes with the reservoir pressure.

1.5.2 Reservoir pressure dynamics for incompressible fluid

We assume that the fluid behaves barotropic, i.e. the density is function of pressure $\rho(p)$. Thus the mass balance in the reservoir is obtained as follows.

$$\frac{\mathrm{d}m_r}{\mathrm{d}t} = V\frac{\mathrm{d}}{\mathrm{d}t}\left(\rho_r(t)\right) = V\frac{\mathrm{d}\rho}{\mathrm{d}p_r}\frac{\mathrm{d}p_r}{\mathrm{d}t} = \dot{m}_{r,in} - \dot{m}_{r,out} \tag{1.28}$$

Employing $\frac{\mathrm{d}p}{\mathrm{d}\rho/\rho} = E$ being E the bulk modulus of elasticity we obtain a first order differential equation for the the reservoir dynamics

$$\dot{p}_r = \frac{E}{\rho V}\left(\dot{m}_{r,in} - \dot{m}_{r,out}\right), \tag{1.29}$$

1.6 Pipeline dynamics

When describing the fluid dynamics inside a pipe, it has been widely accepted to approximate the change of the variables only in one dimension; the longitudinal direction along the pipeline.

The problem is further simplified by neglecting the influence of the gravitation both for gases and liquids. However, we allow wall friction, which will result in pressure loss. In what follows, we derive the governing equations for the fluid dynamics in the pipe for incompressible and compressible cases. The unknown dependent variables along the pipe axial coordinate ξ are density $\rho(\xi,t)$, velocity $v(\xi,t)$, pressure $p(\xi,t)$ and energy $e(\xi,t)$.

1.6.1 Incompressible flow

For incompressible flow we generally assume constant temperature and density. The fluid dynamics is then can be described with the continuity equation and the equation of motion as follows

$$\frac{\partial p}{\partial t} = -a^2\rho\frac{\partial v}{\partial \xi} - v\frac{\partial p}{\partial \xi} \tag{1.30}$$

$$\frac{\partial v}{\partial t} = -\frac{1}{\rho}\frac{\partial p}{\partial \xi} - v\frac{\partial v}{\partial \xi} - \frac{\lambda(\mathrm{Re})}{2D}v|v| \tag{1.31}$$

with λ being the pipe friction coefficient.

1.6.2 Compressible flow

The gas is assumed to be ideal but the change of state is not fixed (i.e. it can be isentropic, isothermic, etc.) hence, besides equations of continuity and momentum balance, we also need to solve an energy-balance equation. We assume that the pipe cross section $A = \text{constant}$ and make an adiabatic pipe approximation (i.e. no heat flux through the wall). Under these assumptions, the dynamical governing equations are

$$\frac{\partial \mathcal{U}}{\partial t} + \frac{\partial \mathcal{F}}{\partial \xi} = \mathcal{Q}, \tag{1.32}$$

with

$$\mathcal{U} = \begin{pmatrix} \rho \\ \rho v \\ \rho e \end{pmatrix}, \quad \mathcal{F} = \begin{pmatrix} \rho v \\ \rho v^2 + p \\ \rho e v + p v \end{pmatrix}, \quad \text{and} \quad \mathcal{Q} = \begin{pmatrix} 0 \\ F_s \\ 0 \end{pmatrix}. \tag{1.33}$$

Now, the overall energy of the gas comprises the sum of its internal internal energy $c_v T$ and kinetic energy $v^2/2$:

$$e(\xi,t) = c_v T(\xi,t) + \frac{v(\xi,t)^2}{2}, \tag{1.34}$$

and, using the ideal gas law we have

$$p(\xi,t) = \rho R T(\xi,t) \tag{1.35}$$

Hence, using these two equations, pressure and temperature can be expressed in terms of the dynamic unknowns v and e.

1.7 Model development, numerical solution techniques

In this section model development of the hydraulic and pneumatic valve systems and numerical techniques for solving their governing equations are presented.

1.7.1 Incompressible model: pipe–valve system

The simplified representation of a hydraulic relief valve connecting to a pipeline is shown in Figure 2.1. The mechanical model consist of a pipeline being enough long to consider the wave effects and a 1 DoF oscillatory system describing the dynamics of the valve body. The diameters of the pipe and the seat are different. The transition between the pipe and the valve is assumed to be an ideal but infinitesimal short diffuser and the flow variables, fluid velocity and pressure are approximated with the help of continuity and Bernoulli's equation along the passage.

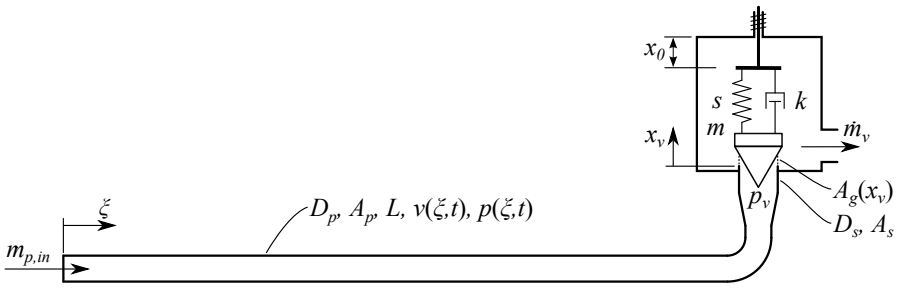

Figure 1.4: Mechanical model of the hydraulic system.

One way to numerically solve the continuity equation and the equation of motion is to approximate the derivatives by finite differences using a staggered grid for pressure and velocity. Staggered grid is used to avoid the so-called 'odd-even coupling' (see **?**) in the pipe. We split the spatial domain in space using a mesh $L = n\Delta l$ $(n = 1, 2, \ldots, N-1)$, where the pressure is stored in the centre of each control volumes and the velocity is located at mesh face. The meshing of the pipe is presented in the Figure 1.5.

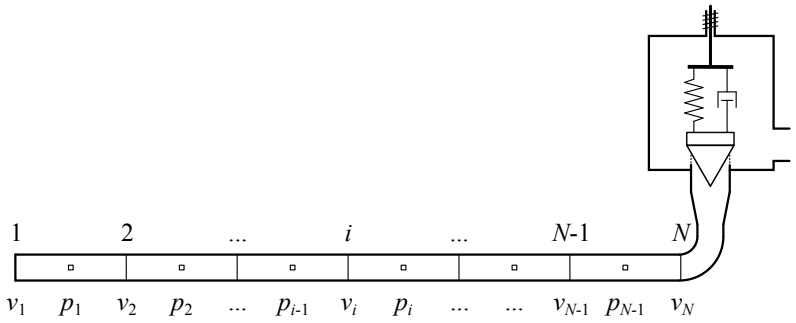

Figure 1.5: Staggered grid of the model. Velocity is stored at mesh faces, while pressure in the centre of mesh.

By discretizing the equation of motion and continuity we obtain

$$\frac{\mathrm{d}v_i}{\mathrm{d}t} = -\frac{1}{\rho}\frac{p_i - p_{i-1}}{\Delta l} - v_i\frac{v_{i+1} - v_{i-1}}{2\Delta l} - \frac{\lambda_e(\mathrm{Re})}{2D_p}v_i|v_i|, \qquad \text{for } i = 2, \ldots, N-1 \tag{1.36}$$

and

$$\frac{\mathrm{d}p_1}{\mathrm{d}t} = -a^2\rho\frac{v_2 - v_1}{\Delta l} - \frac{v_1 + v_2}{2}\cdot\frac{p_2 - p_1}{\Delta l} \tag{1.37}$$

$$\frac{\mathrm{d}p_i}{\mathrm{d}t} = -a^2\rho\frac{v_{i+1} - v_i}{\Delta l} - \frac{v_i + v_{i+1}}{2}\cdot\frac{p_{i+1} - p_{i-1}}{2\Delta l}, \qquad i = 2, \ldots, N-2 \tag{1.38}$$

$$\frac{\mathrm{d}p_{N-1}}{\mathrm{d}t} = -a^2\rho\frac{v_N - v_{N-1}}{\Delta l} - \frac{v_{N-1} + v_N}{2}\cdot\frac{p_{N-1} - p_{N-2}}{\Delta l} \tag{1.39}$$

where v_1 is the velocity in the pipeline at the first mesh point, v_N at the last mesh point. At the first mesh point there is constant inflow, while at the last mesh point we have an equation for the flow through the valve, thus the boundary conditions are

$$v_1 = \frac{Q_{\text{in}}}{A_p} = \text{constant}, \quad v_N = \frac{Q_{v,\text{out}}(x_v, p_v)}{A_p}, \tag{1.40}$$

where p_v is the pressure in front of the valve, $Q_{v,\text{out}}(x_v, p_v)$ can be computed based on (1.11).

The motion of the valve body is modelled as a single degree-of-freedom oscillator as it was introduced in Section 1.4 and given by (1.23), thus the system of differential equations describing the pipe-valve system for $x_v > 0$ is

$$\dot{x}_v = v_v \tag{1.41}$$

$$\dot{v}_v = \frac{F_{fl}}{m} - \frac{s}{m}(x_v + x_0) \tag{1.42}$$

$$\dot{v}_i = -\frac{1}{\rho}\frac{p_i - p_{i-1}}{\Delta l} - v_i\frac{v_{i+1} - v_{i-1}}{2\Delta l} - \frac{\lambda_e(\text{Re})}{2D_p}v_i|v_i|, \qquad \text{for } i = 2, \ldots, N-1 \tag{1.43}$$

$$\dot{p}_1 = -a^2\rho\frac{v_2 - v_1}{\Delta l} - \frac{v_1 + v_2}{2}\cdot\frac{p_2 - p_1}{\Delta l} \tag{1.44}$$

$$\dot{p}_i = -a^2\rho\frac{v_{i+1} - v_i}{\Delta l} - \frac{v_i + v_{i+1}}{2}\cdot\frac{p_{i+1} - p_{i-1}}{2\Delta l}, \qquad \text{for } i = 2, \ldots, N-2 \tag{1.45}$$

$$\dot{p}_{N-1} = -a^2\rho\frac{v_N - v_{N-1}}{\Delta l} - \frac{v_{N-1} + v_N}{2}\cdot\frac{p_{N-1} - p_{N-2}}{\Delta l} \tag{1.46}$$

with the following collision condition for $x_v = 0$

$$(x_v^+,\ v_v^+,\ v_{1,\ldots,N}^+,\ p_{1,\ldots,N-1}^+) = (0,\ -r\,v_v^-,\ v_{1,\ldots,N}^-,\ p_{1,\ldots,N-1}^-), \tag{1.47}$$

being $\square^-$ and $\square^+$ the value of each variable just before and after the impact. In order to assess the required number of the mesh points and thus minimize the error of the solution, we need to compare the solutions for different N. The 'mesh independence' is judged based on the critical flow rate at which the valve looses its stability. Then these critical flow rate values were plotted in function of N in Figure 1.6. It can be observed that the value of the critical flow rate approaches the a distinct value with the increase of number of nodepoints. Based on curve fitting it was shown that the critical flow rate for $N = \infty$ is $Q_{crit,N=\infty} = 19.859\,\ell/\text{min}$. Keeping in mind that larger N values (more grid points) require larger computational effort but more accurate results, $N = 50$ was found to be a reasonable compromise. Still the error is

$$E_{Qcrit} = \left|\frac{Q_{crit,N=\infty} - Q_{crit,N=50}}{Q_{crit,N=\infty}}\right| \times 100\% = \left|\frac{19.859 - 20.133}{19.859}\right| \times 100\% = 1.38\%. \tag{1.48}$$

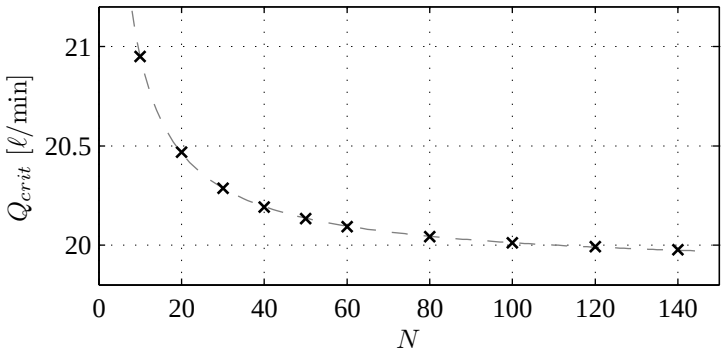

Figure 1.6: Mesh independence study of the distributed parameter system.

1.7.2 Compressible model: reservoir–pipe–valve system

Consider the system depicted in Figure 1.7 consisting of a reservoir, a pipe and a direct spring-loaded valve. The reservoir is taken to be perfectly rigid. The mass flow rate $\dot{m}_{r,\text{in}}$ of the compressible fluid entering the reservoir is presumed either to be constant or to vary slowly when compared to other timescales present in the system. The change of state in the reservoir is assumed to be *isentropic*, that is, there is no heat exchange with the surroundings and there are no internal losses. The mass outflow from the reservoir $\dot{m}_{r,\text{out}}$ is in general assumed to be time varying. The flow in the long, thin pipe is assumed to be captured by one-dimensional unsteady

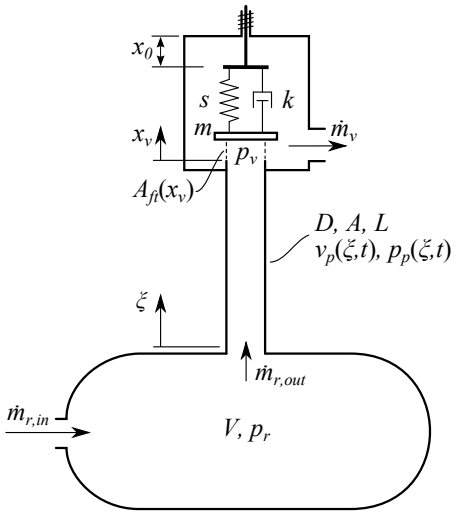

Figure 1.7: Mechanical model of the system.

gas-dynamics theory, including the effects of wall friction. Such an approach captures the inertia of the fluid, its compressibility and pressure losses, which allows for the presence of both wave effects and damping.

The disc shaped valve body can be considered as a degenerated conical valve body of $\alpha = 90°$

half cone angle. A will denote the valve area on which the pressure acts, independent of the valve lift, which for simplicity we take to be equal to the cross-sectional area of the pipe.

Governing equations

The reservoir pressure dynamics for gases is given by (1.27)

$$\dot{p}_r = \frac{a^2}{V}\left(\dot{m}_{r,in} - \dot{m}_{r,out}\right). \tag{1.49}$$

We have solved the GDM using a standard two-step Lax-Wendroff method, as described in e.g. Cebeci et al. (2005); Warren (1983). This is a second-order finite difference scheme of predictor-corrector type. Here we briefly recall the main steps. Let i and j denote the equidistant temporal and spatial grid points:

$$\mathcal{U}_j^i = \mathcal{U}\left(\xi_i, t_j\right), \tag{1.50}$$

with temporal resolution Δt and spatial resolution $\Delta\xi$. The method is comprised of several steps which are set out as follows.

1. Advance $\mathcal{U}_{j+\frac{1}{2}}^{i+\frac{1}{2}}$ at the half time level and middle grid points from

$$\frac{\mathcal{U}_{j+\frac{1}{2}}^{i+\frac{1}{2}} - \mathcal{U}_{j+\frac{1}{2}}^{i}}{\Delta t/2} + \frac{\mathcal{F}_{j+1}^{i} - \mathcal{F}_{j}^{i}}{\Delta\xi} = \frac{\mathcal{Q}_{j+1}^{i} + \mathcal{Q}_{j}^{i}}{2}, \quad \text{where} \quad \mathcal{U}_{j+\frac{1}{2}}^{i} = \frac{\mathcal{U}_{j+1}^{i} + \mathcal{U}_{j}^{i}}{2}.$$

2. Compute the primitive variables (p, ρ, v and e) and find the fluxes $\mathcal{F}_{j+\frac{1}{2}}^{i+\frac{1}{2}}$.

3. Take a full time step to compute $\mathcal{U}_j^{i+1}$ with the help of the centred fluxes $\mathcal{F}_{j+\frac{1}{2}}^{i+\frac{1}{2}}$:

$$\frac{\mathcal{U}_j^{i+1} - \mathcal{U}_j^{i}}{\Delta t} + \frac{\mathcal{F}_{j+\frac{1}{2}}^{i+\frac{1}{2}} - \mathcal{F}_{j-\frac{1}{2}}^{i+\frac{1}{2}}}{\Delta\xi} = \frac{\mathcal{Q}_{j+\frac{1}{2}}^{i+\frac{1}{2}} + \mathcal{Q}_{j-\frac{1}{2}}^{i+\frac{1}{2}}}{2}.$$

For stability, the time step Δt should be small enough to ensure that the 'information' propagating with velocity $a + |v|$ does not 'jump over' a cell. That is,

$$\Delta t < C \min_j \left(\frac{\Delta\xi}{a_j + |v_j|}\right),$$

where $C < 1$ is the safety factor known as the Courrant number and $a_j = \sqrt{\kappa R T_j}$.

Boundary conditions are implemented using of the method of isentropic characteristics, see Zucrow and Hoffman (1976); Cebeci et al. (2005); Warren (1983) for a detailed explanation. Essentially, the technique makes use of the conserved (Riemann) invariant quantities along the characteristic directions:

$$a + \frac{\kappa - 1}{2} v = \text{constant} \quad \text{along} \quad \frac{\mathrm{d}\xi}{\mathrm{d}t} = v + a \quad \text{and} \tag{1.51}$$

$$a - \frac{\kappa - 1}{2} v = \text{constant} \quad \text{along} \quad \frac{\mathrm{d}\xi}{\mathrm{d}t} = v - a. \tag{1.52}$$

The boundary conditions are defined as follows. At $\xi = 0$ we assume isentropic inflow into the pipe. That is, the total enthalpy at the reservoir ($h_r = c_p T_r$) and at the pipe entrance are equal:

$$c_p T_r(t) = c_p T(0,t) + \frac{1}{2}\left(v(0,t)\right)^2, \tag{1.53}$$

which can also be written is terms of pressure, because

$$\frac{T_r}{T_0} = \left(\frac{p_r}{p_0}\right)^z, \quad \text{and} \quad \frac{T(0,t)}{T_0} = \left(\frac{p(0,t)}{p_0}\right)^z, \quad \text{with} \quad z = (\kappa-1)/\kappa. \tag{1.54}$$

At $\xi = L$ we required that the mass flow rate leaving the valve is equal to the mass flow rate within the valve, see (**??**), thus we have

$$\rho(L,t) A v(L,t) = \zeta x_v \sqrt{\rho(L,t) p(L,t)}. \tag{1.55}$$

The equations (1.32)–(1.55) represents a well-posed initial-value problem first-order hyperbolic system of partial differential equations. We refer to this as the full *gas dynamical model* (GDM).

The motion of the valve body is modelled as a single degree-of-freedom oscillator as it was introduced in Section 1.4 and given by (1.23). Since the parameter set of this model is not experimentally tuned, in what follows we assume that the fluid force derives from the pressure only and we neglect the linear momentum change of the fluid and the drag force. The viscous force on the valve body is modelled with some viscous damping k and approximated to be linear function of the valve body velocity. The backpressure behind the valve and due to the relatively high pressure difference between the end of the pipe and the surroundings is considered to be the ambient pressure p_0, the flow through the valve will be assumed to choked. That is, the fluid velocity reaches the local sonic velocity at the annulus cross-section between the disk and the seat and hence backpressure does not affect upstream flow.

Thus the motion of the valve body taking into account the above simplifications is given by

$$m\ddot{x}_v + k\dot{x}_v + s(x_0 + x_v) = \Delta p\, A, \qquad \text{for } x_v > 0, \text{ with } (x_v^+,\ v_v^+) = (0,\ -r v_v^-). \tag{1.56}$$

1.7.3 Tools of quantitative and qualitative analysis

The dynamics of the valve system was studied mainly by performing direct numerical simulations using Runge-Kutta method. The frequency content of the simulations was determined by means of fast Fourier transformation (FFT).

Beside this we were interested at those critical parameter values at which the system looses its stability. The boundary of stability loss was determined with linear stability analysis. Close to the equilibrium the dynamics is governed by the linear coefficient matrix $\mathbf{J}$. The system is stable, if the eigenvalues of $\mathbf{J}$ are less then zero ($Re(\lambda_i) < 0$ for $i = 1, \ldots, n$). If there is a pair of purely imaginary eigenvalues ($Re(\lambda) = 0$, $Im(\lambda) \neq 0$) $\lambda = \pm i\omega$, a Hopf bifurcation exists, the equilibrium loses its stability, a periodic orbit is born (ω is the angular velocity of the self-excited oscillation). A combination of theoretical and computational tools enables prediction of behaviour without the need of direct numerical simulations based at distinct initial conditions. Beside analytical investigations the software AUTO (see Doedel et al. (2009)) is an effective way to explore the dynamics of the valve system. AUTO enables locate and track equilibria or

periodic trajectories, helps to find and follow the linear stability limit the locally bifurcations and determines the eigenvalues.

We were interested in the global dynamics of the valve over the stability loss. The global dynamics was interpreted in two ways, first by means of bifurcation diagrams generated with the help of those points at which the valve body velocity was zero and secondly with the help of AUTO.

Chapter 2

Dynamic instability of a pipe–valve system

2.1 Introduction

The main focus of this chapter is on the analysis of self-excited vibration occurring in a pipe–valve systems (presented in Section **??**), notably on the parametric stability boundaries and the dominant frequency of valve chatter. Thus dynamic measurements were performed for different set pressure values (i.e. spring pre–compression values, x_0), in which, after starting from low flow rates, the revolution number of the screw pump (thus the flow rate) was increased with small steps up to the maximum value (approx. 23 ℓ/min) and then decreased backwards to see if hysteresis occurs. At each flow rate, pressure and displacement time histories were recorded for 4 seconds with 19.2 kHz sampling frequency. This resulted in a total number of 60 measurements per set pressure. Moreover, a distributed parameter system has been developed capable of describing the wave pressure dynamics coupled to the valve body dynamics. Direct numerical simulations and parameter continuation tool was employed for detailed one and two parameter study. Parameters and characteristics of the mathematical model were fitted based on the experiments reported in Chapter **??**. Results of the measurements and simulations were compared good qualitative agreement was found.

The chapter is organised as follows. First in Section **??** we recall the mathematical model of a liquid pipe–valve system based on those governing equations of each element (pipe, valve) that have been introduced in Section 1.7.1. In Section 2.3 a one-parameter study is presented and the global dynamics of the valve is observed as a function of the flow rate. In Section 2.4 a two-parameter study is reported.

2.2 Mathematical model of a pipe–valve system

The model of a pipe–valve system as it was introduced in Section **??** shown in Figure 2.1. The mechanical model consist of a pipeline being enough long to consider the wave effects and a 1 DoF oscillatory system describing the dynamics of the valve body.

The system of ordinary differential equations describing the pipe–valve system consists of two equations for the valve body dynamics, $N-2$ equations for the equation of motion of the fluid in the pipe and N equation for the equation of continuity. Thus the system of ODEs of the

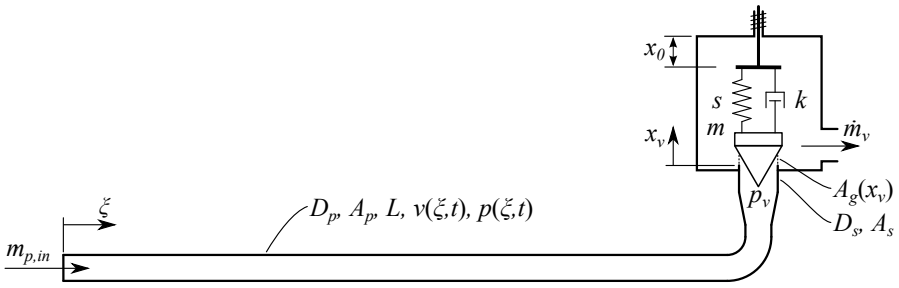

Figure 2.1: Mechanical model of the hydraulic system.

pipe–valve system for $x_v > 0$ is

$$\dot{x}_v = v_v \tag{2.1}$$

$$\dot{v}_v = \frac{F_{fl}}{m} - \frac{s}{m}(x_v + x_0) \tag{2.2}$$

$$\dot{v}_i = -\frac{1}{\rho}\frac{p_i - p_{i-1}}{\Delta l} - v_i\frac{v_{i+1} - v_{i-1}}{2\Delta l} - \frac{\lambda_e(\mathrm{Re})}{2D_p}v_i|v_i|, \qquad \text{for } i = 2,\ldots,N-1 \tag{2.3}$$

$$\dot{p}_1 = -a^2\rho\frac{v_2 - v_1}{\Delta l} - \frac{v_1 + v_2}{2}\cdot\frac{p_2 - p_1}{\Delta l} \tag{2.4}$$

$$\dot{p}_i = -a^2\rho\frac{v_{i+1} - v_i}{\Delta l} - \frac{v_i + v_{i+1}}{2}\cdot\frac{p_{i+1} - p_{i-1}}{2\Delta l}, \qquad \text{for } i = 2,\ldots,N-2 \tag{2.5}$$

$$\dot{p}_{N-1} = -a^2\rho\frac{v_N - v_{N-1}}{\Delta l} - \frac{v_{N-1} + v_N}{2}\cdot\frac{p_{N-1} - p_{N-2}}{\Delta l} \tag{2.6}$$

with the following collision condition for $x_v = 0$

$$(x_v^+,\ v_v^+,\ v_{1,\ldots,N}^+,\ p_{1,\ldots,N-1}^+) = (0,\ -r\,v_v^-,\ v_{1,\ldots,N}^-,\ p_{1,\ldots,N-1}^-), \tag{2.7}$$

being N the number grids along the pipe while $\square^-$ and $\square^+$ the value of each variable just before and after the impact.

2.3 One-parameter study: effect of flow rate at fixed set pressure

Let us start by describing the typical behaviour of the system while varying the flow rate, for a fixed set pressure. The results will be presented by means of bifurcation diagrams as illustrated in the top panel of Figure 2.2, where those displacement values are shown which correspond to zero velocity or impact with the seat.

The bottom panel of the same figure presents the frequency content of the displacement time history. In this plot the appearing frequency is normalised with the pipe eigenfrequency ($f_{p,0} = a/L = 236\,\mathrm{Hz}$). The color intensity of the spectrum demonstrates the displacement amplitude of the evolving vibration in logarithmic scale (red color depicts the high amplitude peaks). Four motion types are highlighted in the top panel, that is (a) highly complex impacting oscillation, (b) regular impacting oscillation, (c) oscillation without impact with the seat, and (d) stable equilibrium. Note that this experimentally obtained diagram is qualitatively similar

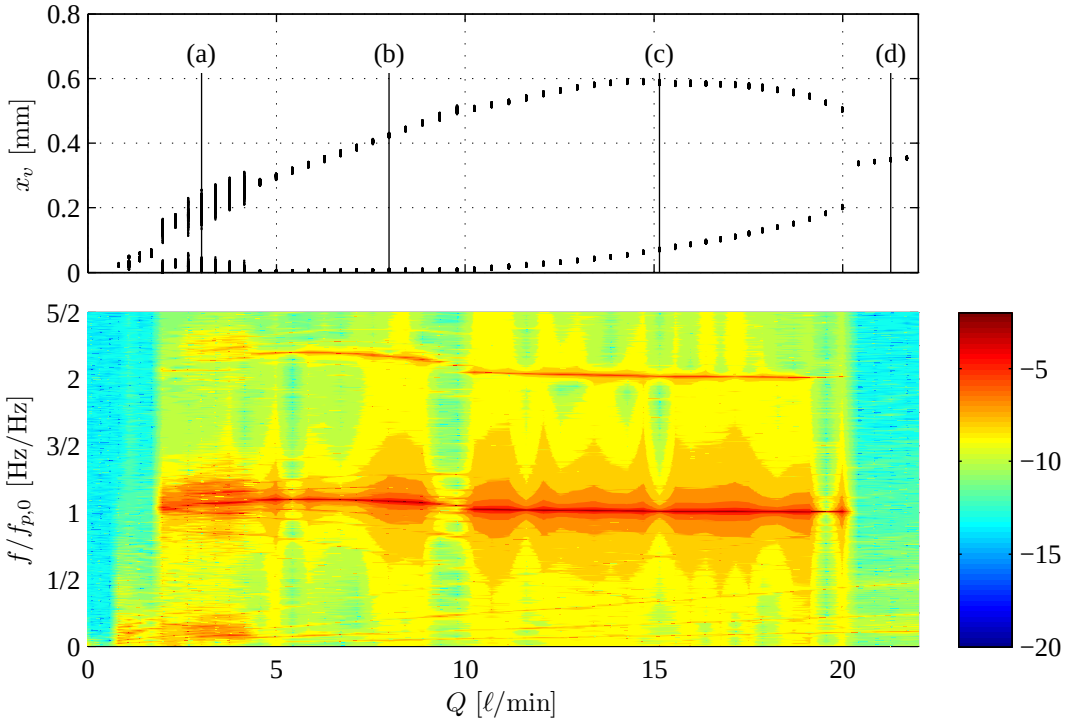

Figure 2.2: Top panel: measured bifurcation diagram showing the behaviour of the system while (slowly) varying the flow rate. Bottom panel: Frequency content of the displacement signal. Spring pre-compression: $x_0 = 17$ mm.

to that one presented by Licskó et al. (2009); Hős and Champneys (2011), which was obtained by numerical modelling. The corresponding displacement and pressure time histories and their spectra are presented in Figure 2.3(a)–2.3(c). In these figures the frequency content is also normalised with the pipe fundamental frequency, the valve mode ($f_v = 27.6\,\mathrm{Hz}$) is represented with gray solid line at $f/f_{p,0} = 0.117$.

As it can be observed in the top panel of Figure 2.2, the valve motion is stable for high flow rates and, upon decreasing the flow, a critical value is reached at 20.4 l/min where the valve looses its stability and chatter appears. As described in Hős and Champneys (2011), the oscillation is born via a Hopf bifurcation, i.e. there is a pair of purely complex eigenvalues of the linearised system. By further decreasing the flow rate, the amplitude of the oscillation grows and, at approx. 14.7 ℓ/min, it reaches the seat and the impacting oscillation regime starts. The point where the valve body first 'grazes' the seat is called a *grazing* bifurcation and is a unique feature of non-smooth dynamical systems, for details see e.g. Di Bernardo et al. (2008). After the grazing bifurcation point the oscillation amplitude decreases with decreasing flow rate. For low flow rates (below 4.15 ℓ/min) we experience highly complex motion form. Finally, at 2.07 ℓ/min the system becomes stable again.

Observing the frequency content of the displacement in the bottom panel of Figure 2.2 it is evident that the dominant frequency in the free-oscillation regime is clearly the pipe eigenfreqency $f_{p,0} \approx 1$ and its second mode. Once the impacting oscillation appears (at approx. 10 ℓ/min.),

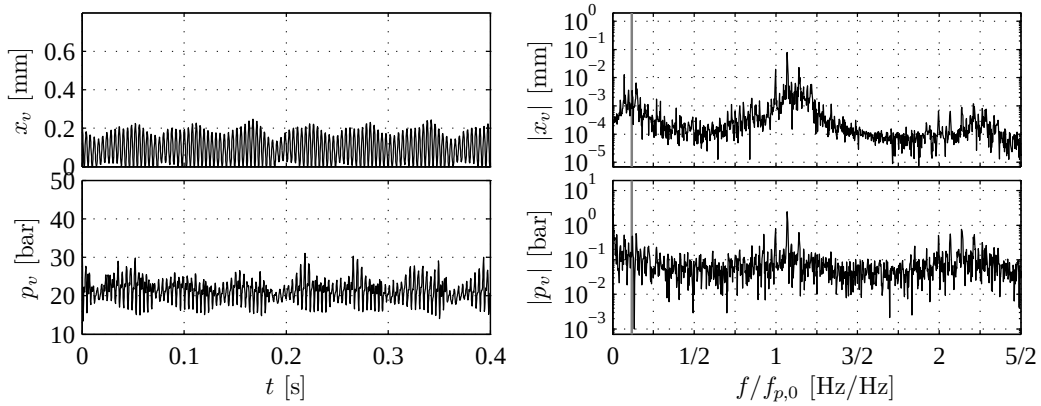

(a) $Q = 3.02\,\ell/\mathrm{min}$

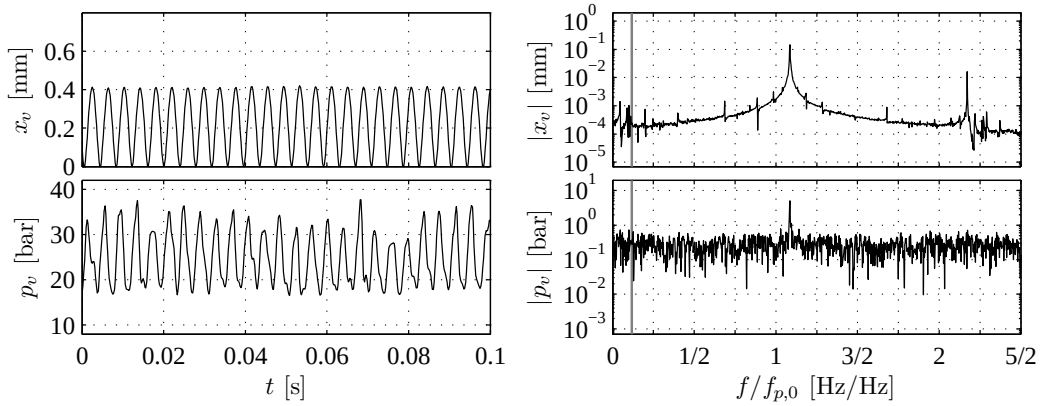

(b) $Q = 7.98\,\ell/\mathrm{min}$

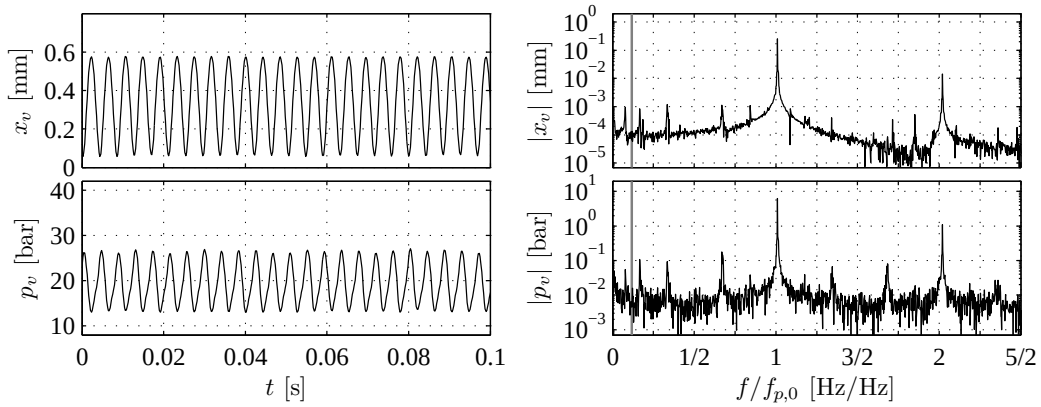

(c) $Q = 15.15\,\ell/\mathrm{min}$

Figure 2.3: Measured valve body displacement and upstream-side pressure time histories and their spectra. Gray solid line depicts the valve eigenfrequency.

there is a slight increase in the frequency, which is caused by the fact that — roughly speaking — the impact interrupts and 'cuts off' a portion of the free oscillation. Having a look at the spectra of the displacement and pressure signals in Figure 2.3(b)–2.3(c) it is striking that the two signals (pressure and displacement) contain essentially the same frequency components.

Let us compare the results with computed ones. Simulations were performed in the same manner as the measurements were carried out, that is the flow rate was decreased from 25 to 0.25 ℓ/min with 0.25 ℓ/min increments. Each simulation was initialised from the previous run. After leaving time the transient to decay 1 s long simulation were run. Then an other series of simulation was ran going from low value of flow rate towards high one to check if hysteresis exists in the dynamics. The resulting bifurcation diagram and the frequency content is presented in Figure 2.4 while displacement and pressure time histories and their spectra is shown in Figure 2.5(a)–2.5(c).

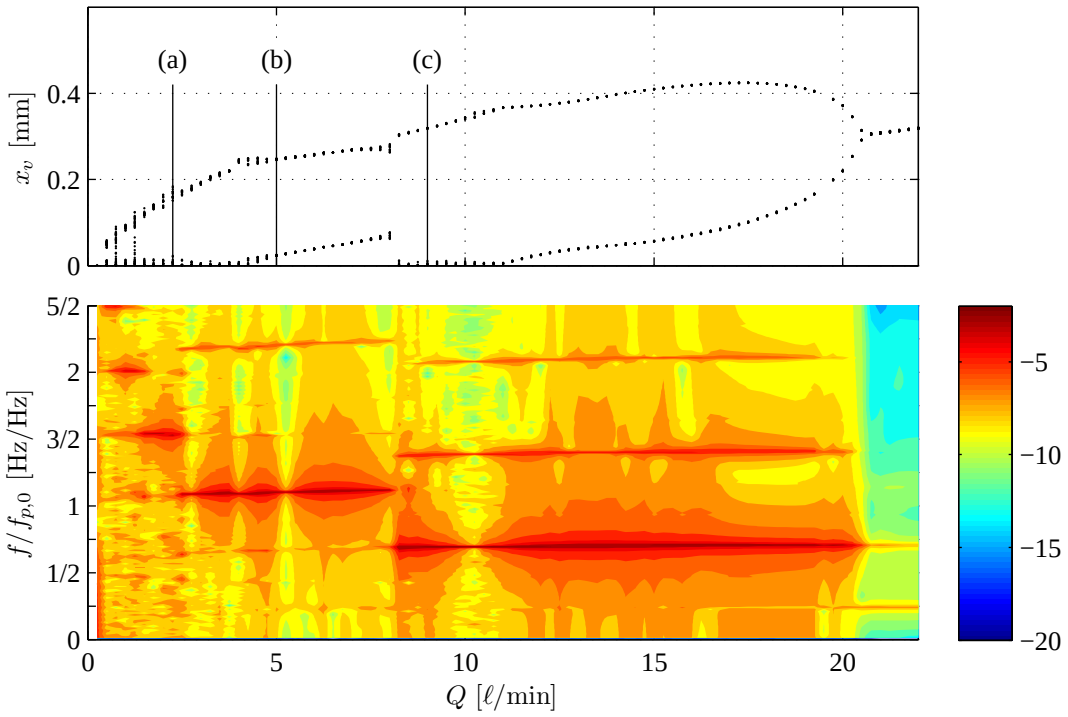

Figure 2.4: Top panel: computed bifurcation diagram showing the behaviour of the system while (slowly) varying the flow rate. Bottom panel: Frequency content of the displacement signal. Spring pre-compression: $x_0 = 17$ mm.

As it can be seen the dynamics is very similar to the one obtained experimentally. For high values of the flow rate the valve remains at its equilibrium position meanwhile no wave effects occur in the pipe. Decreasing the flow rate the equilibrium loses its stability via Hopf bifurcation; impact-free oscillation born. Further decreasing the flow rate the valve grazes at 11 ℓ/min. Contrary to experiments, after a sudden transition the motion form becomes again impact-free oscillating up to 4.25 ℓ/min from where again impacting vibration can be observed. The map of the frequency content reveals that the transition is a consequence of pipe mode

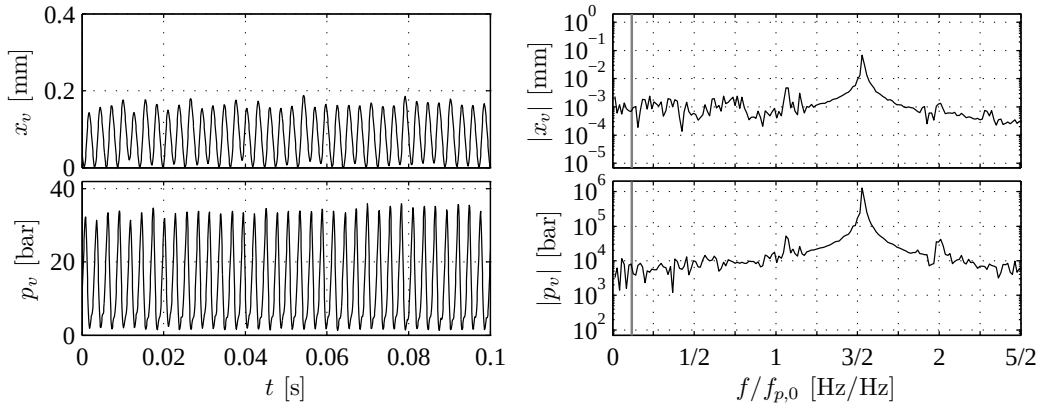

(a) $Q = 2.25\,\ell/\mathrm{min}$

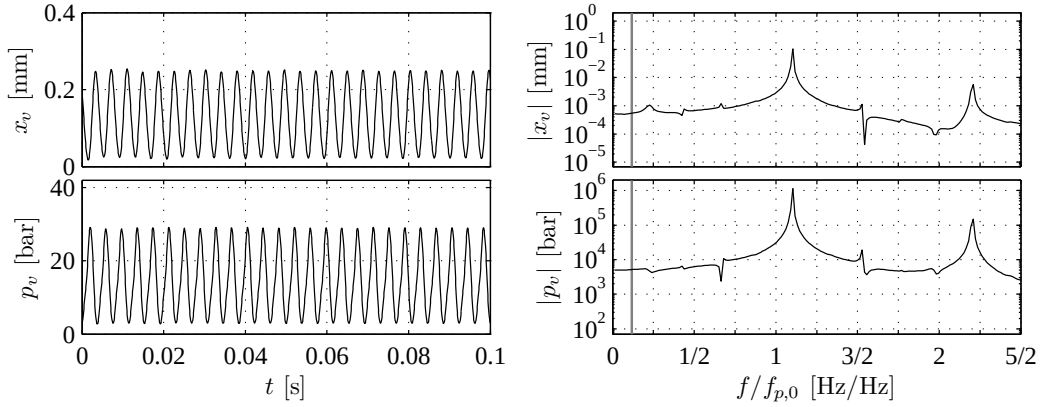

(b) $Q = 5\,\ell/\mathrm{min}$

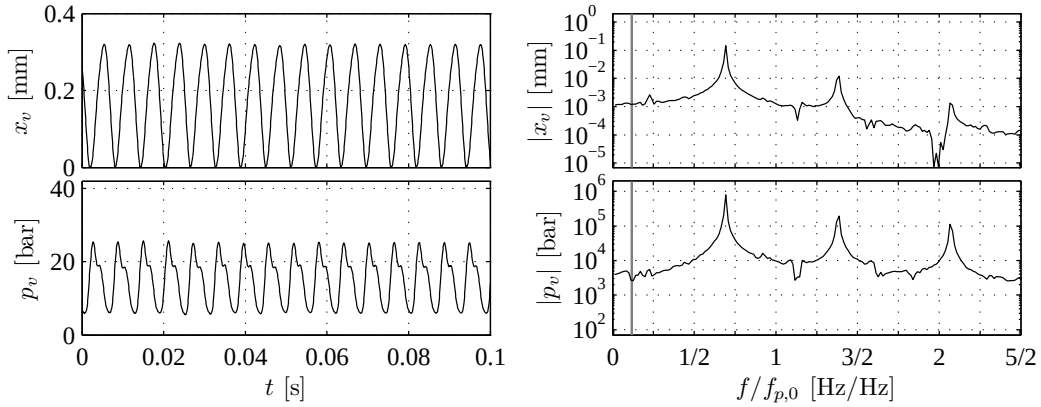

(c) $Q = 9\,\ell/\mathrm{min}$

Figure 2.5: Computed valve body displacement and upstream-side pressure time histories and their spectra. Gray solid line depicts the valve eigenfrequency.

switching. For high flow rates for example $f/f_{p,0} = 3/4$ and its higher modes dominate the pipe dynamics. The first switching occurs at 11 ℓ/min from where the characteristic mode corresponds to a wave ($f/f_{p,0} = 1$) followed by the second mode switching at 3.5 ℓ/min to $f/f_{p,0} = 3/2$. Although this transition was not observed in the experiments reported above the phenomenon has already been experienced by Hayashi (1995) and Botros et al. (1997). Both studies indicated that several modes can exist at the same pipe length and concluded that to determine which mode occurs in the pipe is highly non-trivial. The possible wave length of the standing waves can be $\frac{(n+1/2)}{2}L$, for $n = 0, 1, 2, \ldots$. Contrary to measurement, valve mode is not present in the spectrum obtained by simulation.

2.4 Two-parameter study: effect of set pressure

Next, let us present the effect of set pressure by analysing the bifurcation diagrams obtained by setting different spring pre-compression. Up to $x_0 = 13\,\text{mm}$ the valve remained stable for the entire flow rate regime. Beyond $x_0 = 13.5\,\text{mm}$ we experienced self-excited vibrations. To explore the dynamics of the valve in $Q - x_0$ parameter plane measurements were conducted by varying the flow rate for a set of spring pre-compression. Figure 2.6 demonstrates the variation of the valve body dynamics for several pre-compression values. Appendix?? exhibits the bifurcation diagrams and frequency map for all the measured pre-compression level.

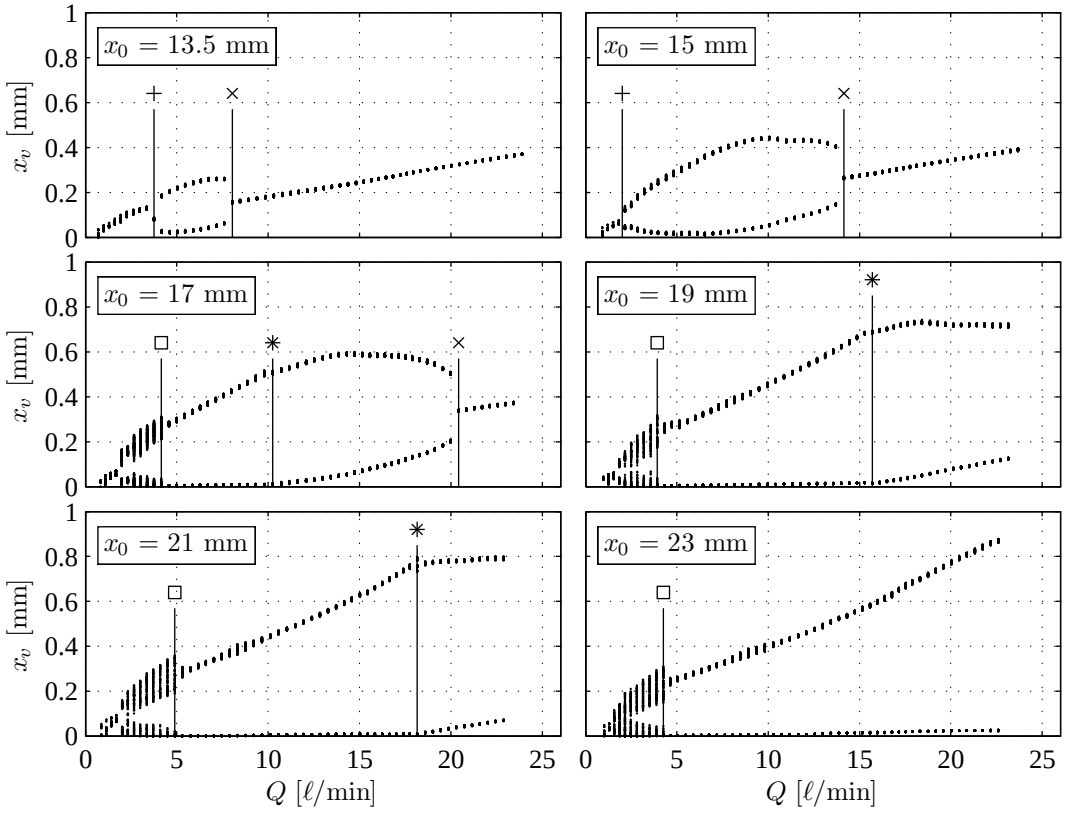

Figure 2.6: Measured bifurcation diagrams for different spring pre-compression values.

First, notice that upon increasing the set pressure, the point of the initial instability denoted by cross is also increasing, i.e. the unstable region increases. For low pre-compressions ($x_0 = 13.5$ and 15 mm) we observe a second critical flow rate, below which the motion stabilizes. Note, this point was not captured by the model in Hős and Champneys (2011). For higher set pressures, this point becomes hard to identify, and it is also unclear if it persists or is destroyed.

The same mechanism applies for the rest of the regimes: the chaotic and the impacting regimes also become wider. In the case of the last three set pressures, no stable valve motion was experienced neither at high, nor at low flow rates.

The appearing frequency at the primary stability loss is listed in Table 2.1. For a given set pressure value, this frequency remained constant up to the occurrence of impacting oscillations, as already shown in Figure 2.2 and Table 2.1. We emphasise again that these frequencies are very close to the pipe eigenfrequency, which is $f_{p,0} = 236\,\mathrm{Hz}$.

x_0 [mm]	Q [ℓ/min]	f [Hz]
13.5	8.033	244.9
14	10.69	243.2
14.5	12.44	241.4
15	14.15	239.7
15.5	15.36	239.7
16	17.28	237.9
17	20.42	237.9

Table 2.1: Critical flow rate and oscillation frequency at the initial stability loss.

Finally, we present the essence of the measurements in Figure **??**, where all the previously described special points are depicted on the $Q{-}x_0$ plane. These points in the order of appear upon decreasing the flow rate are the primary Hopf bifurcation ($\times$), grazing bifurcation $*$, secondary Hopf bifurcation $+$, and the point of at which the pipe-valve dynamics coupling first occurs ($\square$). The points of the primary and secondary Hopf bifurcation determine the boundary of loss of stability. This boundary is demonstrated with dashed line in Figure **??**. Below the stability boundary the equilibrium is stable while above it the above mentioned motion forms exist. Effort has been made to compute the stability boundary with AUTO; its result is illustrated with solid line in the figure. The computed stability boundary shows qualitative agreement with the measured one, however, for $Q > 2.89\,\ell$/min the model over predicts while below $2.89\,\ell$/min under predicts the measurement. Focusing on the experimentally obtained results, it can be concluded that the range of unstable operation widen upon increasing the spring pre-compression as placement of the primary ($\times$) and secondary ($+$) Hopf bifurcation moves towards high and low flow rate values. The rate of change of the dislocation is nearly linear for both cases; in the case of primary Hopf bifurcation its value is $dQ/dx_0 \approx 3.54\,{}^{\ell/\mathrm{min}}/_{\mathrm{mm}}$ while in the case of secondary Hopf bifurcation it is $dQ/dx_0 \approx -0.653$. Let us quantify the change. For $x_0 = 13.5\,\mathrm{mm}$ the equilibrium is unstable for $3.7521\,\ell/\mathrm{min} < \mathrm{Q} < 8.033\,\ell/\mathrm{min}$. Pre-compressing the spring by 14.8 % to $x_0 = 15.5\,\mathrm{mm}$ involves a 302 % increase in the unstable operation range of the flow rate (the equilibrium is unstable between 2.45 and $15.36\,\ell$/min). The region of the impacting oscillation ($*$) increases in a similar intense manner while the pipe-valve dynamics coupling ($\square$) occurs approximately at the same flow rate.

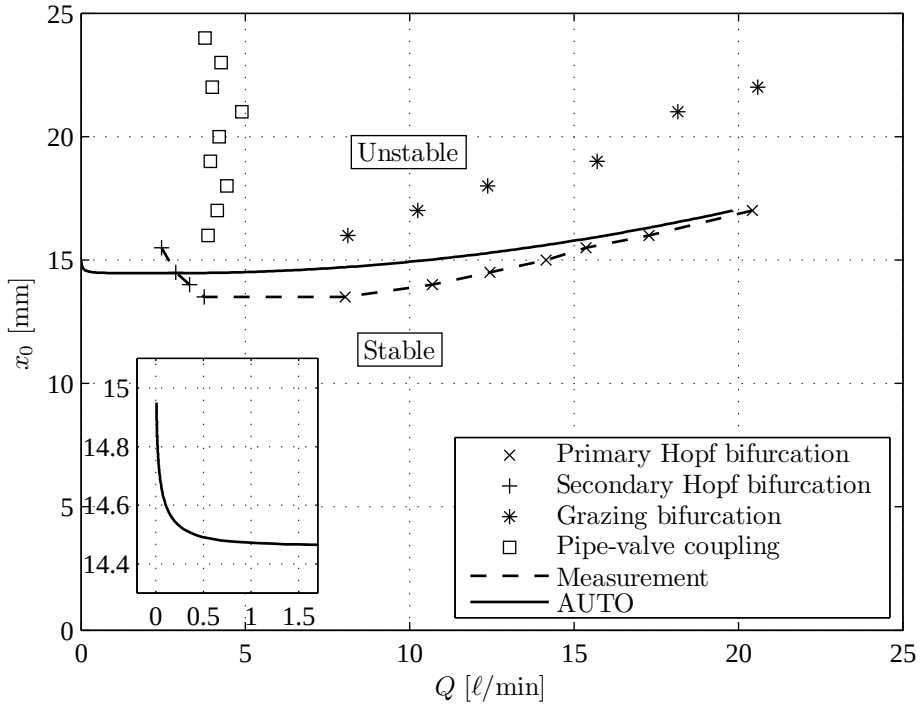

Figure 2.7: Boundary of loss of stability obtained experimentally (dashed line) and with AUTO (solid line) and the experienced motion types. $\times$ and $+$ stand for the primary and secondary Hopf bifurcation, $*$ depicts the point at which the valve body first impacts the seat (grazing bifurcation) while $\square$ presents the points at which pipe-valve dynamics coupling first occurs upon decreasing the flow rate.

2.5 Conclusion

A systematic experimental study was presented on relief valve instability for slightly compressible fluid (hydraulic oil). The experimental system consisted of a positive displacement pump, a simple direct spring loaded valve and a hydraulic hose connecting them. Pressure and displacement time histories were recorded for a large number of flow rates and set pressures.

We have experimentally validated the qualitative bifurcation diagram given by Hős and Champneys (2011). The experiments show that for high flow rates, the valve equilibrium is stable, which, upon decreasing the flow rate, looses its stability via a Hopf bifurcation. A free, non-impacting oscillation is born, whose amplitude increases with decreasing the flow rate and once the valve body reaches the seat impacting periodic orbit is born, whose amplitude decreases with decreasing flow rate. At low flow rates, pipe-valve dynamics coupling was observed. Finally, for very low flow rates, the valve stabilizes again, but only for low set pressures. Upon increasing the set pressure the unstable regime expands quickly and vice versa: a critical set pressure can be found, below which the valve is stable for all flow rates.

An interesting outcome of our study was that although the experimental results qualitatively agreed with the 'no-pipe-model' presented by Hős and Champneys (2011), the oscillation

frequency remained constant for a wide parameter range (both in terms of flow rate and set pressure). Moreover, this frequency coincides with the pipe eigenfrequency $f_{p,0} = a/L$, which suggests that the initial valve stability loss (Hopf bifurcation) immediately couples with the pipe's internal dynamics and the latter dominates the behaviour of the system.

From a more practical point of view it was clearly seen that there is a critical spring pre-compression below which the valve is unconditionally stable. Qualitatively explaining, the higher the spring pre-compression is, the smaller the valve openings are and the more intense the acoustical feedback inside the pipe is (see Misra et al. (2002)). This critical spring pre-compression can be found by simple linear stability analysis during the design phase.

2.6 Contribution

Olyan matematikai modellt alkottam egy csővezeték és az ahhoz kapcsolódó kúpos zárótestű nyomáshatároló szelep dinamikus modellezésére, mely alkalmas az ilyen rendszerekben előforduló instabilitások nemlineáris dinamikai vizsgálatára. A modell segítségével lehetővé válik az instabil paramétertartományok hatékony meghatározása lineáris stabilitásvizsgálat alkalmazásával, valamint a globális dinamika vizsgálata. Mérések segítségével bizonyítottam a modell gyakorlati alkalmazhatóságát.

Bibliography

Askari, E., Jeong, K.-H., Amabili, M., 2013. Hydroelastic vibration of circular plates immersed in a liquid-filled container with free surface. Journal of Sound and Vibration 332 (12), 3064 – 3085.
URL http://www.sciencedirect.com/science/article/pii/S0022460X13000096

Botros, K., Dunn, G., Hrycyk, J., 1997. Riser-relief valve dynamic interactions. Journal of Fluids Engineering 119, 671.
URL http://fluidsengineering.asmedigitalcollection.asme.org/article.aspx?articleid=1428478

Cebeci, T., Shao, J. P., Kafyeke, F., Laurendeau, E., 2005. Computational fluid dynamics for engineers: from panel to Navier-Stokes methods with computer programs. Springer.

Di Bernardo, M., Budd, C., Champneys, A., Kowalczyk, P., 2008. Piecewise-smooth dynamical systems: theory and applications. Vol. 163. Springer Verlag.

Doedel, E., Champneys, A., Dercole, F., Fairgrieve, T., Kuznetsov, Y., Oldeman, B., Paffenroth, R., Sandstede, B., Wang, X., Zhang, C., 2009. Auto: Software for continuation and bifurcation problems in ordinary differential equations. Tech. rep., Concordia University, Montreal.
URL http://cmvl.cs.concordia.ca/auto/

Hayashi, S., 1995. Instability of poppet valve circuit. Japan Society of Mechanical Engineers International Journal. Ser. C, Dynamics, Control, Robotics, Design and Manufacturing 38 (3), 357–366.
URL http://ci.nii.ac.jp/naid/110004089461/en/

Hős, C., Champneys, A. R., 2011. Grazing bifurcations and chatter in a pressure relief valve model. Physica D: Nonlinear Phenomena 241 (22), 2068 – 2076.
URL http://www.sciencedirect.com/science/article/pii/S0167278911001229

Kasai, K., 1968. On the stability of a poppet valve with an elastic support : 1st report, considering the effect of the inlet piping system. Bulletin of Japan Society of Mechanical Engineers 11 (48), 1068–1083.
URL http://ci.nii.ac.jp/naid/110002361294/en/

Khalak, A., Williamson, C., 1997. Fluid forces and dynamics of a hydroelastic structure with very low mass and damping. Journal of Fluids and Structures 11 (8), 973–982.
URL http://www.sciencedirect.com/science/article/pii/S0889974697901109

Licskó, G., Champneys, A., Hős, C., 2009. Nonlinear analysis of a single stage pressure relief valve. International Association of Engineers International Journal of Applied Mathematics 39 (4), 1–14.

Misra, A., Behdinan, K., Cleghorn, W. L., 2002. Self-excited vibration of a control valve due to fluid-structure interaction. Journal of Fluids and Structures 16 (5), 649 – 665.
URL http://www.sciencedirect.com/science/article/pii/S088997460290441X

Takenaka, T., 1964. Performances of oil hydraulic control valves. Bulletin of Japan Society of Mechanical Engineers 7 (27), 566–576.
URL http://ci.nii.ac.jp/naid/110002363102/

Urata, E., 1969. Thrust of poppet valve. Bulletin of The Japan Society of Mechanical Engineers 12 (53), 1099–1109.
URL http://ci.nii.ac.jp/naid/110002361394/

Warren, M, D., 1983. Appropriate boundary conditions for the solution of the equations of unsteady one-dimensional gas flow by the lax-wendroff method. International Journal of Heat and Fluid Flow 4 (1), 53–59.
URL http://www.sciencedirect.com/science/article/pii/0142727X83900279

Zucrow, M. J., Hoffman, J. D., 1976. Gas dynamics. Vol. 1. New York: John Wiley and Sons, 1976.